



ELSEVIER

Available online at [www.sciencedirect.com](http://www.sciencedirect.com)

SCIENCE @ DIRECT®

Earth and Planetary Science Letters 238 (2005) 204–216

EPSL

[www.elsevier.com/locate/epsl](http://www.elsevier.com/locate/epsl)

# The interaction between the post-perovskite phase change and a thermo-chemical boundary layer near the core–mantle boundary

Takashi Nakagawa<sup>a,\*</sup>, Paul J. Tackley<sup>b,c</sup>

<sup>a</sup>*Department of Earth and Planetary Sciences, University of Tokyo, Japan*

<sup>b</sup>*Department of Earth and Space Sciences, University of California, Los Angeles, USA*

<sup>c</sup>*Institute of Geophysics and Planetary Physics, University of California, Los Angeles, USA*

Received 4 February 2005; received in revised form 28 June 2005; accepted 29 June 2005

Available online 15 August 2005

Editor: S. King

## Abstract

Numerical simulations of thermo-chemical mantle convection with the newly-discovered post-perovskite (PPV) phase change are used to characterize its dynamical consequences for the D" region, which has frequently been interpreted as being thermo-chemical in origin. A strong lateral variation in the appearance of the PPV region is observed, with high CMB temperatures leading to "double-crossing" of the phase boundary in average or cold regions, or no crossing in hot regions. Lower CMB temperatures result in a single crossing everywhere but with highly variable depth. The strongly exothermic nature of the post-perovskite phase change induces an anti-correlation between regions containing a thick PPV layer and piles of chemically dense material formed by the segregation of the crustal component from subducted slabs. The PPV phase change destabilizes chemically-dense material, allowing subducted slabs to easily penetrate into a dense layer, forming isolated patches of the post-perovskite phase. Whereas the lateral spectrum of thermal anomalies in the deep mantle is dominated by long wavelengths, the lateral spectrum of composition is relatively flat and is the dominant contributor to seismic velocity variations at all wavelengths except the very longest ones.

© 2005 Elsevier B.V. All rights reserved.

*Keywords:* post-perovskite phase change; double-crossing; thermo-chemical structures; D" region

## 1. Introduction

Three proposed origins for the highly heterogeneous structures in the CMB region observed in

various seismological studies are (1) compositional, (2) thermal, and (3) phase change related. Regarding composition, several global tomographic studies (e.g., [1,2]) have indicated that compositional variations are necessary to explain large-scale, high amplitude structures in the deep mantle, possibly consistent with numerical models of thermo-chemical mantle convection in which 'piles' of dense

\* Corresponding author. Tel.: +81 3 5841 8332; fax: +81 3 5841 8791.

E-mail address: [takashi@eps.s.u-tokyo.ac.jp](mailto:takashi@eps.s.u-tokyo.ac.jp) (T. Nakagawa).

material form underneath large-scale upwellings [3–5]. On the other hand, to explain the “Lay” discontinuity observed at the top of D” in many areas and the negative velocity gradient below this, Sidorin et al. [6] found, by comparing synthetic seismograms calculated for various numerical convection models with data, that a strongly exothermic phase transition deflected by temperature variations fits the observations better than a chemical boundary. Thus, the preferred explanation of deep mantle structure probably involves both compositional variations and an exothermic phase change interacting with temperature variations. Previously this explanation had the problem that no suitable phase change was known, but recently a phase change from perovskite to a post-perovskite (PPV) phase, expected to take place at approximately 2700 km depth, was discovered and investigated [7,8]. This new phase change is strongly exothermic, with a Clapeyron slope in the range +8 to +10 MPa K<sup>-1</sup> [8,9]. Due to its strongly positive Clapeyron slope combined with the large temperature gradients that are expected in the thermal boundary layer above the CMB, it has been proposed that a second (“double”) crossing of the phase change back to the perovskite stability field occurs several tens of kilometers above the CMB, and that such a feature has been found in the Eurasia region by comparing real data with synthetic seismograms generated for such a “double-crossing” scenario [10–12].

A numerical modeling study of the effect of this phase change on purely thermal mantle convection [13] indicated that it destabilizes the lower boundary layer, resulting in a greater number of small-scale boundary-layer instabilities (leading to plumes) and a warmer mantle interior. However, that exploratory study lacked certain features that are thought to be important in mantle dynamics, particularly compositional variations in the deep mantle, and variable viscosity with plate-like lithospheric behavior. Thus, the modeling is here extended to include these complexities. In this study, numerical simulations of thermo-chemical mantle convection in a two-dimensional cylindrical shell are used to investigate the relationship and interaction between chemically-dense material and the PPV phase boundary in the CMB region. The present study focuses on questions such as: (1) What is the spatial relationship

between the PPV phase change and possible compositional ‘piles’? (2) How does the PPV phase change affect the stability of dense material above the CMB? (3) Which structures best fit the seismological data?

## 2. Model

The numerical code STAG3D is used to study thermo-chemical mantle convection in a two-dimensional cylindrical shell (e.g., [14]) with the radii of the CMB and surface boundaries rescaled such that surface area ratios match those in spherical geometry [15]. The compressible anelastic and infinite Prandtl approximations are made, as usual. The physical properties density, thermal expansivity, and thermal diffusivity are assumed to be dependent on depth, as given in [14]. Phase changes are incorporated at 400 km (+2.5 MPa K<sup>-1</sup>) and 660 km (–2.5 MPa K<sup>-1</sup>) in addition to the deep mantle PPV phase change. The version of the model used here is presented in great detail including all relevant equations in [20,21]. The only major change is made because of the large PPV Clapeyron slope and the possibility of crossing the PPV phase boundary twice or not at all [10], which makes it important to use a numerical phase change treatment that allows these possibilities and correctly includes phase change deflection, rather than one in which the phase change is assumed to occur at a fixed depth. Thus, a phase function approach, based on that in [16], is used:

$$\begin{aligned} \Gamma_{\text{ppv}}(T, d) \\ = 0.5 + 0.5 \tanh \left( \frac{d - d_{\text{ppv}} - \gamma_{\text{ppv}}(T - T_{\text{ppv}})}{w} \right) \end{aligned} \quad (1)$$

where  $\Gamma_{\text{ppv}}$  is the phase function for post-perovskite, which varies from 0 for perovskite to 1 for post-perovskite,  $T$  and  $d$  are temperature and depth, respectively,  $(T_{\text{ppv}}, d_{\text{ppv}})$  is a point on the phase boundary,  $\gamma_{\text{ppv}}$  is the Clapeyron slope and  $w$  is the width of the phase transition, which for numerical reasons must be taken to be wider than realistic. The values of these parameters are given in Table 1. The energy equation is identical to that given in previous studies (e.g., Eq. (3) of [20,21]) but it is instructive

Table 1  
Physical parameters for the post-perovskite phase change

Symbol	Meaning	Dimensional values
$\Delta\rho_{\text{ppv}}$	Density jump	66.4 kg m <sup>-3</sup>
$\gamma_{\text{ppv}}$	Clapeyron slope	0, +8, +16 MPa K <sup>-1</sup>
$T_{\text{ppv}}$	Temperature at phase boundary	2650 K
$d_{\text{ppv}}$	Depth at phase boundary	2700 km
$w$	Width of phase boundary	30 km

The density jump is calculated by using experimental data Murakami et al. [7].

to reproduce it here because the latent heat term is affected by the post-perovskite transition:

$$\begin{aligned} \bar{\rho}\bar{c}_p \left[ \frac{\partial T}{\partial t} + \mathbf{u} \cdot \nabla T \right] = & -Di_s \bar{\alpha} \bar{\rho} T u_r + \nabla \cdot (\bar{k} \nabla T) \\ & + \bar{\rho} R_h + \frac{Di_s}{Ra} \tau_{ij} u_{i,j} \\ & + \bar{c}_p \frac{Di_s T}{\bar{\rho}} \sum_{i=1}^{\text{n phase}} P_i \frac{d\Gamma_i}{dz} u_r \quad (2) \end{aligned}$$

where the barred quantities  $\bar{\rho}$ ,  $\bar{c}_p$ ,  $\bar{\alpha}$  and  $\bar{k}$  are radius-dependent reference state properties density, heat capacity, thermal expansivity and thermal conductivity respectively, the calculation of which is defined in Eqs. (11) to (14) of [3].  $Di_s$  is the surface dissipation number,  $Ra$  is the Rayleigh number defined using reference (generally surface) parameters,  $\mathbf{u}$  is velocity,  $R_h$  is internal heating rate and  $\tau_{ij}$  is the stress tensor. In the last (latent heat) term,  $P_i$  is the conventional phase buoyancy parameter for the  $i$ th phase change and  $\Gamma_i$  is the phase function for the  $i$ th phase change.  $\Gamma$  for the post-perovskite transition is given above and its form for the other two transitions is given in [20,21]. The technical implementation of phase changes in STAG3D has been discussed in detail in [3,14,20,21]. To summarize: a different reference state is calculated for each phase, and the properties in a particular grid cell (most importantly, reference density) depend on the relative fraction of the different phases as given by the appropriate phase functions. In order to avoid possible numerical problems associated with the last term in (2) when  $\Gamma_i$  changes rapidly, the advection step is performed on potential temperature rather than total temperature, as potential temperature is not changed by phase transitions or adiabatic heating/cooling so has a much simpler energy equation. Potential tempera-

ture is then transformed to actual temperature to compute other terms in (2).

The viscosity is temperature-, depth- and yield stress-dependent, given by

$$\begin{aligned} \eta_d(T, z) = & \eta_0 [1 + (\Delta\eta - 1)H(z - 0.223)] \exp[4.6z] \exp \left[ \frac{27.631}{T + 1 - T_s} \right] \\ \sigma_Y(z) = & \sigma_b + \sigma_d z \\ \eta(T, z, \dot{\epsilon}) = & \min \left( \eta_d(T, z), \frac{\sigma_Y(z)}{2\dot{\epsilon}} \right) \end{aligned} \quad (3)$$

where  $\eta_d(T, z)$  is the ductile viscosity,  $\Delta\eta$  is the viscosity jump between the upper and lower mantles,  $H$  is the Heaviside step function,  $\sigma_Y(z)$  is the depth-dependent yield stress,  $\sigma_d$  is the yield stress gradient,  $\sigma_b$  is the yield stress at the surface,  $\dot{\epsilon}$  is the second invariant of the strain rate tensor,  $T_s$  is the surface temperature and  $z$  is the vertical coordinate, which varies from 1 at the CMB to 0 at the surface. In this formulation, the viscosity changes by six orders of magnitude with temperature, two orders of magnitude with depth (although the increase along an adiabat is less), and  $\Delta\eta=10$  across the 660 km discontinuity. Since material properties of perovskite and post-perovskite (i.e., elasticity and thermodynamical properties) are similar [17,18], it does not appear necessary to include a viscosity jump at this phase transition.

Some notable recent studies have included the temperature-dependence of thermal conductivity in addition to the pressure-dependence included here, including [29] who also included the post-perovskite phase change. Here, in order to not introduce too many complexities at once, we focus on the combined effect of compositional variations and the post-perovskite phase transition and leave temperature-dependent thermal conductivity to a future study.

Compositional variations are assumed to arise from melt-induced differentiation, which is treated in the same manner as in previous studies [19–21], i.e., by comparing, after each timestep, the local temperature to a depth-dependent solidus (shown in Fig. 1 of [19]). When the temperature in a cell exceeds the solidus, the fraction of melt necessary to bring the temperature back to the solidus is generated and instantaneously placed at the surface to form crust, then the cell temperature is set back to the solidus [20]. Composition is represented by the variable  $C$ , which varies from 0 (harzburgite) to 1 (basalt/eclogite). The density

contrast between these extremes is here taken to be constant with depth for simplicity.

Radioactive heating is included and is enhanced by a factor of ten in the dense material, to crudely account for the partitioning of incompatible heat-producing elements into the oceanic crust. Thus:

$$R_h(C, t) = H_0 \left( \frac{1 + 9C}{1 + 9\langle C \rangle} \right) \exp((t_a - t) \ln 2 / \tau) \quad (4)$$

where  $H_0$  is the present-day heating rate in the regular mantle,  $t_a$  is the age of the Earth (4.5 Gyr),  $t$  is the time since the beginning of the calculation and  $\tau$  is the average half-life of radiogenic heating, taken to be 2.43 Gyr. The average present-day internal heating rate in the mantle is set to 23.7 in the non-dimensional equations, corresponding to a dimensional value of  $6.2 \times 10^{-12} \text{ W kg}^{-1}$ .

The boundary conditions at the top and bottom boundaries are impermeable and shear stress free for velocity, isothermal for temperature and zero mass flux for composition. The side boundaries are periodic. The bottom thermal boundary condition accounts for cooling of the core, and is given by  $dT_{\text{CMB}}/dt = -KF_{\text{CMB}}$  where  $T_{\text{CMB}}$  is CMB temperature, which is initially set to 4200 K,  $K$  is the cooling coefficient given as

Table 2

Physical mantle parameters

Symbol	Meaning	Non-dimensional value	Dimensional value
$Ra_0$	Rayleigh number	$1 \times 10^7$	N/A
$d$	Thickness of the mantle	1	2890 km
$\eta_0$	Reference viscosity	1	$1.4 \times 10^{22} \text{ Pa s}$
$\rho_0$	Reference (surface) density	1	$3300 \text{ kg m}^{-3}$
$g$	Gravity	1	$9.8 \text{ m s}^{-2}$
$\alpha_0$	Reference (surface) thermal expansivity	1	$5 \times 10^{-5} \text{ K}^{-1}$
$\kappa_0$	Reference (surface) thermal diffusivity	1	$7 \times 10^{-7} \text{ m}^2 \text{ s}^{-1}$
$\Delta T_{\text{sa}}$	Temperature scale	1	2500 K
$T_s$	Surface temperature	0.12	300 K
$\sigma_b$	Yield stress	$10^5$	117 MPa
$\sigma_d$	Yield stress gradient	$4 \times 10^5$	$162.4 \text{ Pa m}^{-1}$

$$Ra_0 = \rho_0 \alpha_0 \Delta T_{\text{sa}} d^3 / \kappa_0 \eta_0.$$

$K = 3\rho_m c_m d / \rho_c c_c r_{\text{CMB}}$  (e.g., Steinbach et al. [22]), and  $F_{\text{CMB}}$  is the CMB heat flow given by the thermo-chemical mantle convection calculation. A numerical grid of 256 (horizontal)  $\times$  128 (vertical) cells is used, with an average of 16 tracers per grid cell to track the composition. This grid results in  $\sim 25$  km vertical grid spacing, with 13 cells in the D''

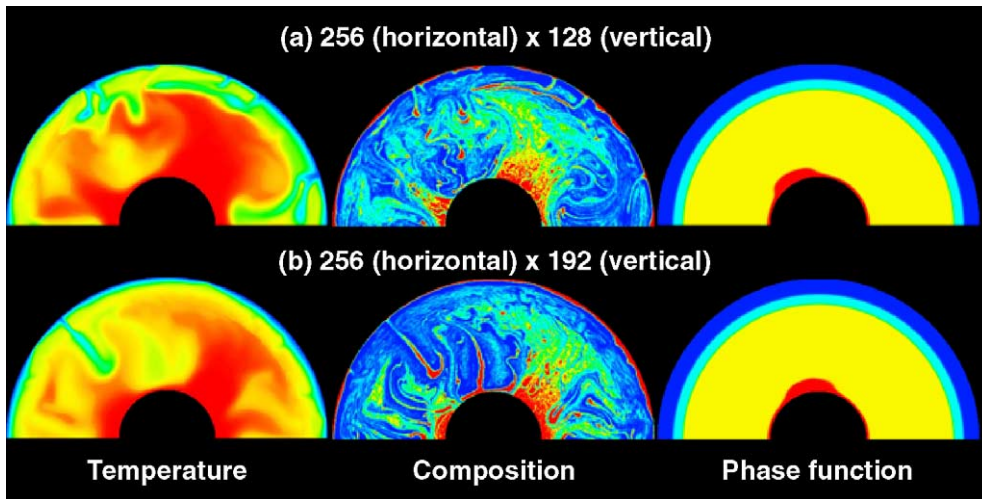


Fig. 1. Comparison of identical cases with different numerical resolutions: (a) the standard resolution ( $256 \times 128$ ) and (b) higher vertical resolution ( $256 \times 192$ ), which has approximately 15 km vertical spacing. The cases have a PPV Clapeyron slope of  $+8 \text{ MPa K}^{-1}$  and a 2% density difference between basaltic and hartzburgitic material. The general character and statistical nature of the temperature, composition and phase function fields are quite similar to each other, indicating that the original resolution is sufficient for characterizing such structures in the CMB region.

region, i.e., the 300 km directly above the CMB. In the horizontal direction, 256 cells gives a grid spacing of  $\sim 14$  km at the CMB. As a resolution test, an identical case was computed but with 192 vertical cells (compared in Fig. 1). The qualitative similarity of chemical and phase-change features between these calculations indicates that the standard resolution is sufficient to resolve the features investigated in this study. Although this calculation includes a quantitative description of the thermal evolution of the Earth's core, we focus on the interaction between the PPV phase change and thermochemical convection; the thermal evolution of the core in this situation will be addressed in another paper. The physical parameters for the mantle used in this study are listed in Table 2. Cases are started from an initial condition in which the temperature field is adiabatic (potential temperature, 1600 K) with thin error function thermal boundary layers at the top and the bottom plus small

random perturbations, and the compositional field is initialized at a constant  $C=0.3$ .

In order to investigate the relationship between compositional variations and the PPV phase change, the most important parameter of each is varied, namely density contrast and Clapeyron slope, respectively. The density difference between subducted MORB and pyrolite in the deep mantle is quite uncertain. Thus, we test three plausible values for the density change between  $C=0$  harzburgite and  $C=1$  MORB: 0%, 2% and 3% of the reference (surface) density, i.e., 0, 66 or 99  $\text{kg m}^{-3}$ . These correspond to values of the chemical buoyancy parameter  $B = \Delta\rho_c / \rho_0 \alpha_0 \Delta T_{\text{sa}}$  of 0, 0.16 and 0.24. In order to clearly elucidate the effect that the post-perovskite phase change is having, we test not only the predicted value of 8  $\text{MPa K}^{-1}$  but also zero, and twice the predicted value, i.e., 16  $\text{MPa K}^{-1}$ , here referred to as “exaggerated”. This leads to a total of nine cases.

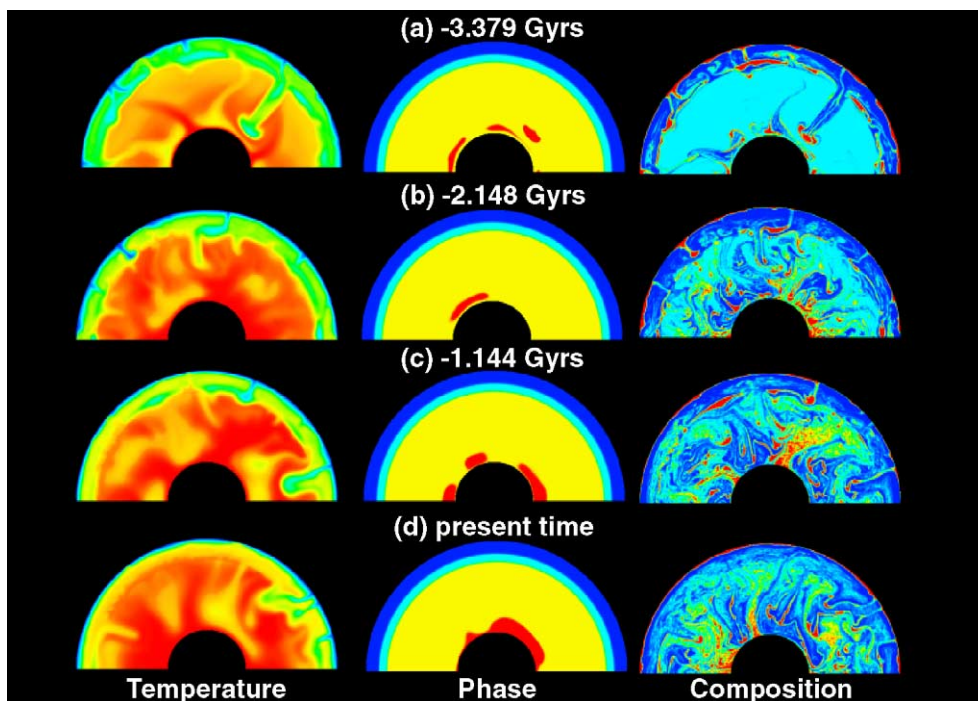


Fig. 2. The time evolution of temperature (left), phase function (center) and composition (right) fields for the case with an exaggerated (+16  $\text{MPa K}^{-1}$ ) Clapeyron slope and a 2% compositional density variation. The fields are plotted at (a) 3.379 Gyrs before present, (b) 2.148 Gyrs before present, (c) 1.144 Gyrs before present, and (d) the present day, i.e., after 4.5 Gyrs of model evolution. The temperature field is colored from hot (red) to cold (blue). For the phase function, blue is olivine, sky blue is spinel, yellow is perovskite and red is post-perovskite. Composition varies between basaltic (red) and harzburgitic (blue).



### 3. Results

#### 3.1. Time evolution

The time evolution of the thermo-chemical structure and phase boundaries for the case with a 2% compositional density variation and the exaggerated value of the PPV transition ( $16 \text{ MPa K}^{-1}$ ) is illustrated in Fig. 2. The evolution of the composition and temperature fields is similar to that in previous models that have continuous crustal differentiation (e.g., [19–21]), with a highly heterogeneous structure developing over billions of years, although with this 2% density contrast subducted crust is not able to form a long-term stable layer above the CMB. At early times, convection is somewhat layered, with the upper mantle becoming depleted (blue) more rapidly than the lower mantle.

The plots of ‘phase’ show the locations of different mineralogies: blue=olivine, cyan=spinel, yellow=perovskite, red=post-perovskite. At early times, when the core is hot enough that the CMB temperature and pressure is in the perovskite stability field, some features predicted by [10] are observed: (i) post-perovskite occurs in a “sandwich”, with perovskite above and below, and (ii) it does not blanket the entire CMB, because in regions where the mantle is hot the geotherm does not pass through the PPV stability field. Furthermore, at the earliest time illustrated (Fig. 2a) an isolated patch of PPV is visible some distance from the CMB within the base of a cold ‘avalanche’. With increasing time the core cools, leading to a pinching off of the near-CMB perovskite region (Fig. 2c) until eventually the PPV phase extends to the CMB and occurs everywhere (Fig. 2d). Even with a ubiquitous boundary, however, the

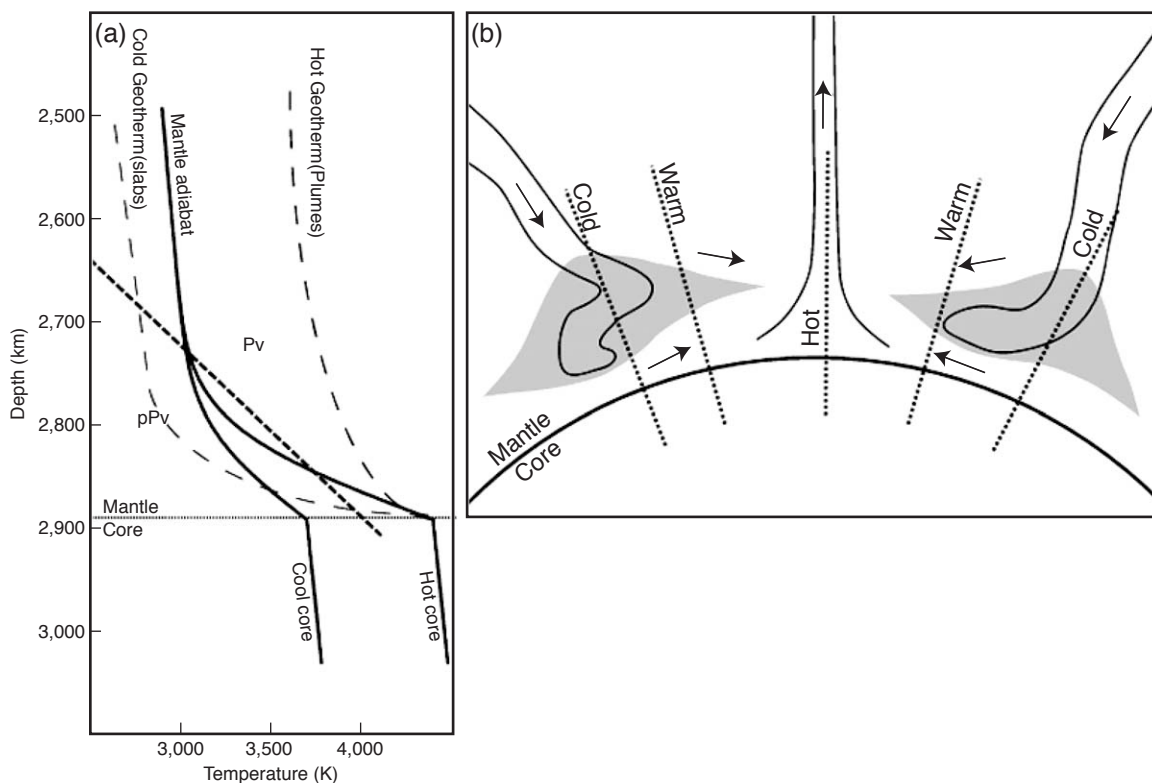


Fig. 3. A schematic interpretation of post-perovskite structures observed in Fig. 1. (a) Relationship between various geotherms (solid and long dashed lines) and the PPV phase boundary (short dashed line). (b) The relationship between PPV regions and thermal features for a hot core scenario, reproduced from Hernlund et al. [10] with permission (see <http://www.nature.com/nature/journal/v434/n7035/full/nature03472.html>).

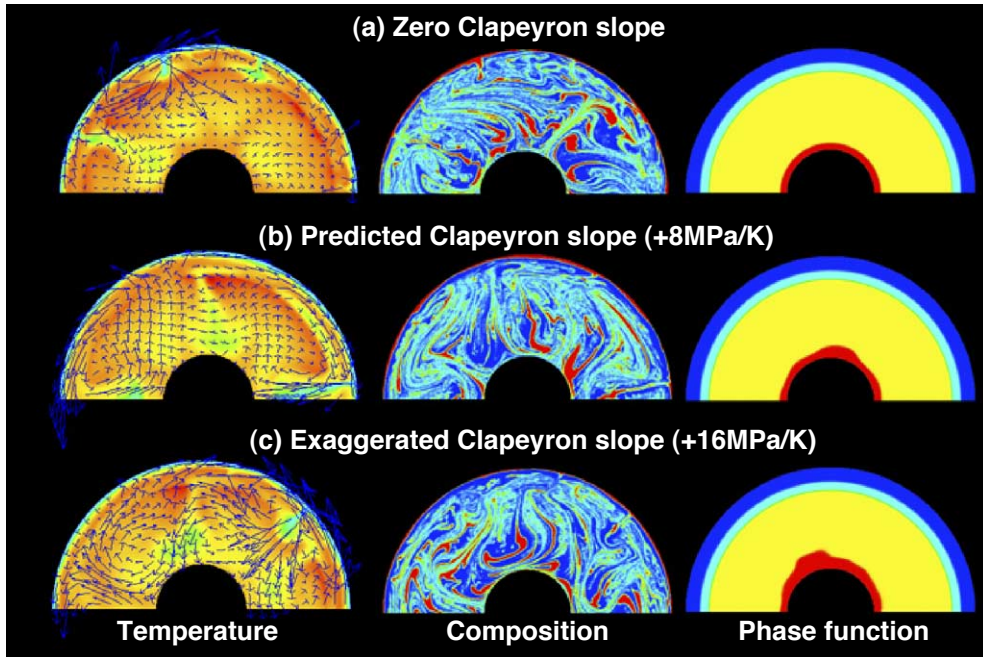


Fig. 4. (a–c) Temperature, phase and composition fields for cases with zero compositional density variation. Colors as in Fig. 1. Blue arrows indicate velocity.

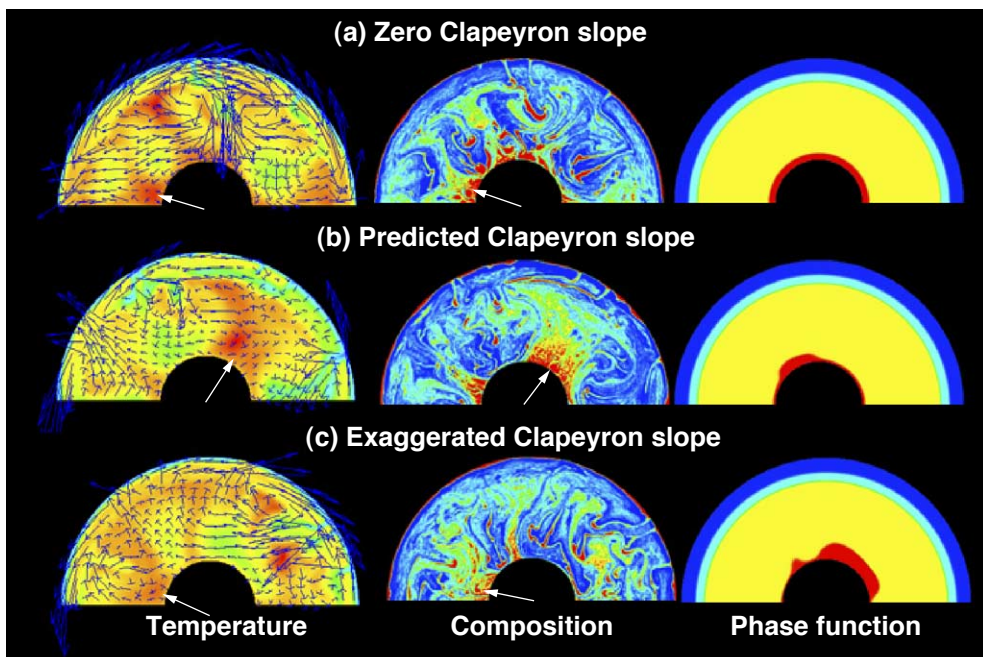


Fig. 5. (a–c) Temperature, phase and composition fields for cases with a 2% compositional density difference. Colors and blue arrows as in Fig. 1. White arrows indicate the position of small-scale flow inside the dense piles or layer.

topography is considerable, with a very thin PPV layer in hot regions but thick layer in cold regions. As dense segregated subducted crust is swept towards upwellings (see Fig. 2d), there is an anticorrelation between regions where a thick PPV layers exists, which are where cold subducted slabs accumulate, and regions where piles of subducted crust build up.

Fig. 3 (from [10]) illustrates how these different structures may be explained by different geotherms interacting with the phase diagram, with geotherms plotted in Fig. 3a and schematic structures for a hot core scenario illustrated in Fig. 3b. Thus for a hot CMB that is in the perovskite stability field, the average mantle adiabat may result in a double crossing and a PPV sandwich, while a cold region (e.g., a slab reaching the CMB) will experience a thicker sandwich, and a hot region (e.g., an upwelling plume) may miss the PPV stability field altogether, i.e., have zero crossings. The reason for a transition from double- or zero-crossing to a single crossing as the CMB temperature is decreased is also clear from Fig. 3a.

### 3.2. Dependence on compositional density variation and Clapeyron slope

Fig. 4 shows thermo-chemical structures for cases with zero chemical density variation and the three values of Clapeyron slope, after 4.5 billion years of evolution. As expected, subducted crust does not settle above the CMB but is instead passively stretched and folded by the flow. In all cases the core has cooled sufficiently that a continuous layer of PPV is formed above the CMB, which is flat in the case of zero Clapeyron slope. The PPV layer becomes thicker with increasing Clapeyron slope, indicating greater cooling of the core and deep mantle. The phase boundary is shallow in regions where cold slabs reach the CMB region and deep in hot regions, as previously discussed.

With a 2% chemical density difference and zero Clapeyron slope (Fig. 5a), subducted oceanic crust can settle into a messy layer covering the CMB. However, with the Clapeyron slope increased to the predicted value (Fig. 5b), such a layer is not stable and instead the dense material is swept into piles under-

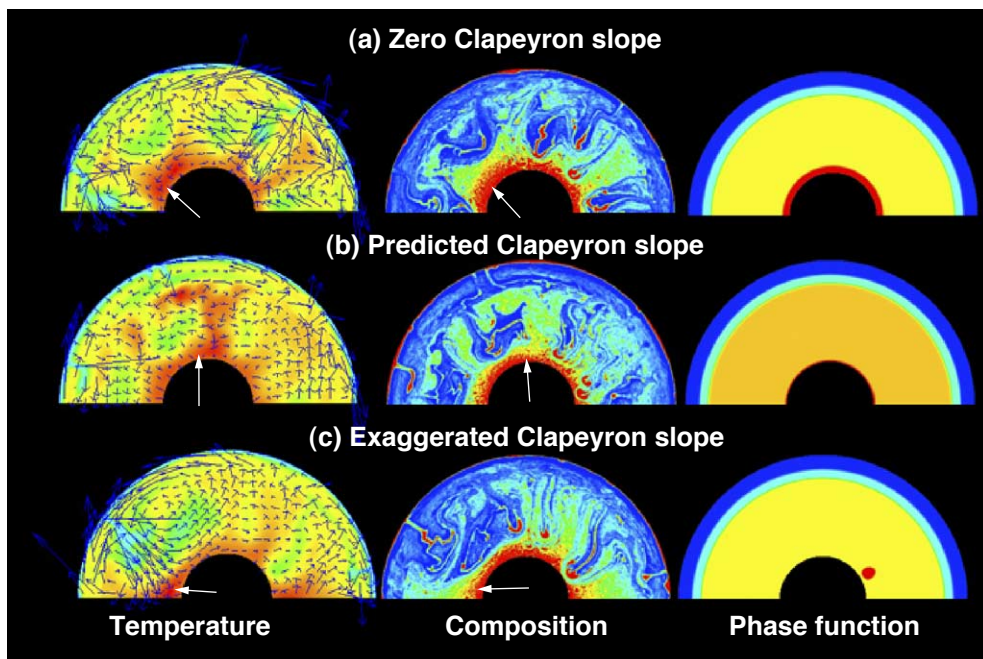


Fig. 6. (a–c) Temperature, phase and composition fields for cases with a 3% compositional density difference. Colors and blue arrows as in Fig. 1. White arrows indicate the position of small-scale flow inside of the dense piles or layer.



neath the upwelling regions. When the Clapeyron slope is doubled (Fig. 5c), any deep layering becomes even more tenuous. These results indicate that the exothermic PPV phase transition destabilizes the thermo-chemical boundary layer above the CMB. They also further illustrate the anticorrelation between places with a thick PPV layer and places with piles of dense material. Regarding core cooling, there is a competition between two effects: reduction of the cooling rate by blanketing of the core by a dense layer (e.g., [19]) and increased cooling rate due to the PPV transition [13].

With a 3% chemical density difference (Fig. 6), a layer of dense subducted crust forms above the CMB regardless of the strength of the PPV transition. This dense, radioactive heating enriched material makes the CMB region hot, so that when the Clapeyron slope is as predicted (Fig. 6b), only a very thin PPV layer is formed, and with an exaggerated Clapeyron slope (Fig. 6c), PPV is localized to the tip of a subducted slab. The formation of a PPV patch in the tip of a slab gives it an additional negative buoyancy that helps it to penetrate deeper towards the CMB.

Fig. 7 shows the mantle geotherms for each density variation and Clapeyron. With a 0% chemical density variation (Fig. 7a), the mantle geotherms for cases with a positive post-perovskite Clapeyron slope are slightly cooler than for a zero Clapeyron slope, which seems to contradict our previous results [13] in which this phase change resulted in a warmer mantle. These results can be reconciled by considering the thermal evolution aspect, which was missing in our previous study: The post-perovskite phase change causes higher CMB heat flow so that the core becomes cooler, which also reduces lower mantle temperatures. An additional mechanism arises from melting: If the mantle starts hotter then more melting occurs, which can rapidly reduce the temperature.

With a 2% or 3% chemical density variation (Fig. 7b and c), geotherms for positive Clapeyron slope cases are typically higher than those for zero Clapeyron slope cases, except in the deepest mantle where a layer may form. This is because the presence of a dense basaltic layer results in higher temperatures inside the layer and lower temperatures above the layer, and adding the post-perovskite phase change reduces this layering, causing more of the heat-producing element enriched material to be entrained.

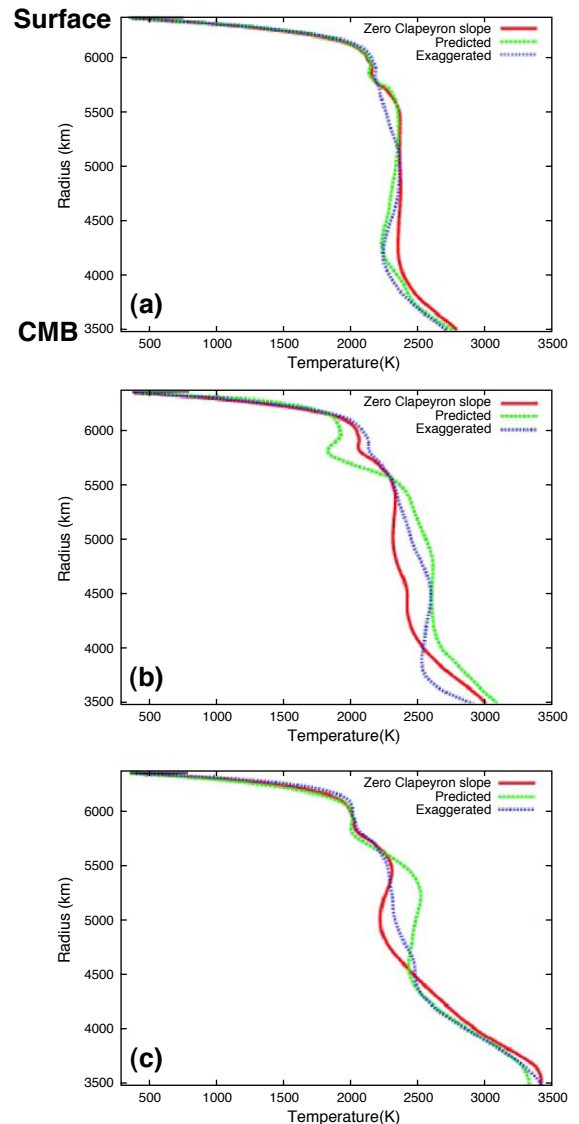


Fig. 7. Radial temperature profiles. (a) 0% chemical density difference, (b) 2% chemical density difference and (c) 3% chemical density difference.

### 3.3. Implications for seismic structure in the CMB region

It is useful to convert model thermal and compositional anomalies to seismic velocity anomaly, in order to compare to constraints from global seismic tomography models (e.g., [1,2]). As in our previous paper [5], composition is converted to iron fraction using

$X_{Fe} = 0.05 + 0.1C$ , and scaling factors from  $X_{Fe}$  or temperature to seismic shear wave velocity are taken from [2].

Here we focus on the lateral spectra of shear wave velocities at 2700 km depth, which are plotted for the different cases in Fig. 8. With a zero Clapeyron slope (Fig. 7a), large amplitude, low degree (i.e., long wavelength) structure is observed. However, as the compositional density contrast is increased to 2% then 3%, this low-degree structure decreases in amplitude, leading to a flatter spectrum. In order to understand why this is happening, the contributions of temperature and composition to the spectrum are plotted separately (Fig. 8d and g, respectively). The temperature spectrum is barely influenced by the compositional density contrast and is very red, decreasing strongly with increasing

degree. In contrast, the spectrum of composition is much flatter, presumably because small-scale variations that would be generated by the compositional effects (see white arrows shown in Figs. 4a and 5a for instance) are not erased by diffusion as with the thermal field, and changes dramatically with compositional density contrast. Comparing these individual spectra with the total spectra (Fig. 8a), it is clear that composition dominates except perhaps at the very longest wavelengths.

When the predicted Clapeyron slope is used (Fig. 8b, e, h) the same characteristics and trends are observed. This is presumably because the PPV transition destabilizes the dense material. When the Clapeyron slope is further increased (Fig. 8c, f, i) the 3% density contrast case also becomes more similar to the other cases.

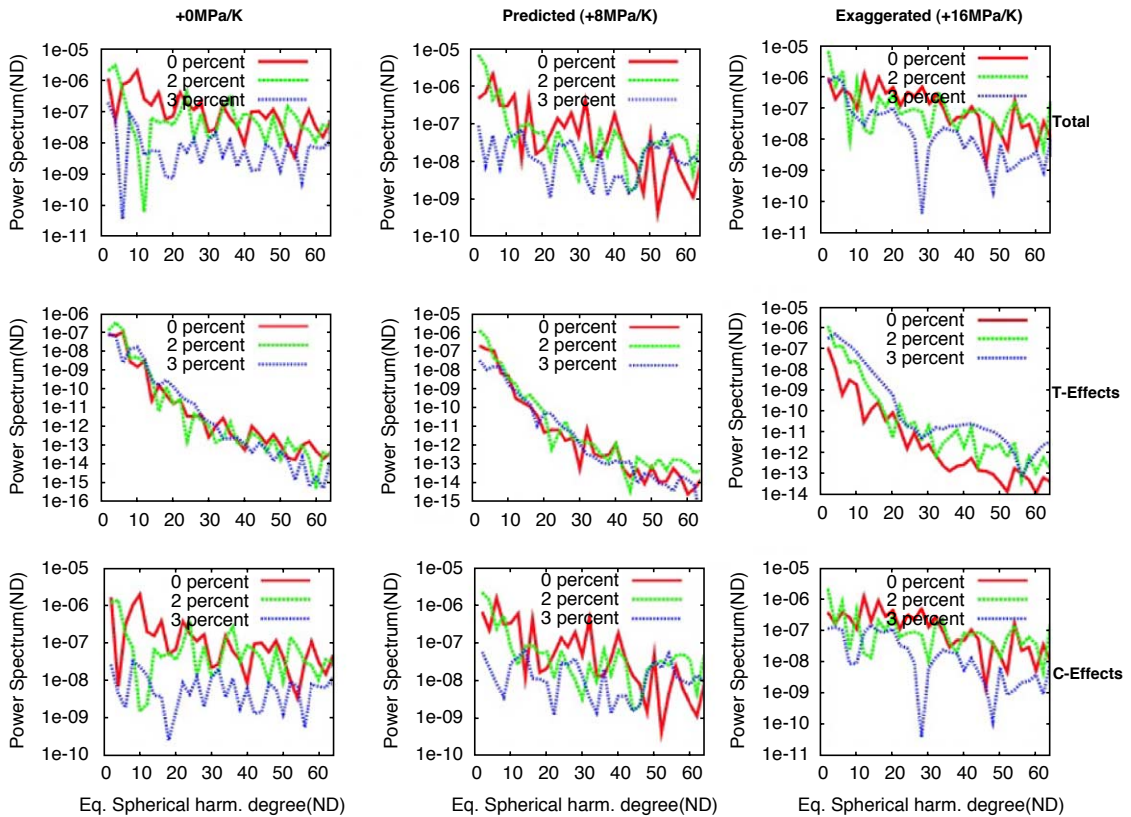


Fig. 8. Lateral spectra of calculated seismic shear wave velocity anomalies at 2700 km depth. Top row: total spectra (assuming both temperature and compositional anomalies) for (a) zero Clapeyron slope, (b) predicted Clapeyron slope and (c) exaggerated Clapeyron slope. Middle row: Spectra calculated using temperature only (d) zero, (e) predicted, (c) exaggerated. Bottom row: Spectra calculated using composition only (g) zero, (h) predicted, (f) exaggerated Clapeyron slope.

These results suggest that the formation of a stable layer of dense material above the CMB causes a decrease in lateral heterogeneity compared to cases with no layering (0% density contrast) or semi-stable “piles” (2% or 3% density contrast). The main effect of the PPV transition is to alter the density contrast at which this change in planform takes place. It should be noted that for these spectra, PPV is assumed to have the same seismic velocity as perovskite, which is probably not realistic [16,23]. If PPV were assumed to have a different  $V_s$ , then lateral variations in the PPV region would add an additional contribution to the spectrum, which must be evaluated in future studies.

These results also suggest that the contribution of compositional variations to seismic wave variations is far larger than the contribution of temperature variations, which is consistent with recent seismological constraints on mantle structure [2,24]. There is some uncertainty in the conversion factors between the model  $C$  field and  $X_{\text{Fe}}$  and between  $T$  or  $X_{\text{Fe}}$  and  $V_s$ , but the differing slopes of the thermal and compositional spectra guarantees that composition will dominate at shorter wavelengths.

#### 4. Conclusions and discussion

In this study, the interaction between the post-perovskite phase transition and thermo-chemical structures in the CMB region is investigated using a numerical model of thermo-chemical mantle convection. The major findings are:

- (1) A zero-, single- or double-crossing of the PPV phase boundary can occur depending on the temperatures of the CMB and deep mantle.
- (2) Regions where a thick PPV layer exists are anticorrelated with piles of dense material, because the vertical temperature profile through the hot dense piles may not intersect the PPV stability field at all (if the CMB is in the perovskite stability field) or crosses it very close to the CMB (if the CMB is in the PPV stability field).
- (3) If a stable dense layer covers the entire CMB, then the transition to PPV may not occur at all (if the CMB is in the perovskite stability field) or occurs very close to the CMB (if the CMB is in the PPV stability field).
- (4) A thick post-perovskite layer is typically found in regions where subducted slabs pool above the CMB, and sometimes isolated patches of post-perovskite are found in the tips of downwelling slabs as they approach the CMB region.
- (5) The post-perovskite phase change destabilizes dense material above the CMB, such that a larger chemical density contrast is needed to stabilize layering or piles.
- (6) Whereas temperature has a “red” lateral temperature spectrum that decreases rapidly with increasing degree, the spectrum of composition is relatively flat, guaranteeing that composition is the dominant contributor to seismic wave velocity at short wavelengths and possibly even at long wavelengths.
- (7) A stable layer of dense material results in lower amplitude long-wavelength structure than passive composition or marginally-stable dense piles.

Recent analysis of seismograms (i.e., using waveform fitting between real data and synthetic seismograms) has indicated that, in the Eurasia area and Caribbean Sea area, features consistent with double-crossing of the PPV phase boundary are found [10–12]—namely, two seismic discontinuities in the lowermost mantle, with a positive change in seismic velocity for the shallower one and a negative change in seismic velocity for the deeper one. This implies that the CMB is in the perovskite stability field, i.e., hotter than in the models presented here after 4.5 Gyr evolution. Improvements in our model such as a more sophisticated treatment of heat balance in the core [19] and a higher initial core temperature, would most likely result in a higher, presumably more realistic present-day CMB temperature, and should be investigated in the future.

Several other aspects of the model could be made more realistic in the future, including: (1) a proper treatment of a pyrolite-like mantle composition (e.g., [25–27]), i.e., including non-olivine phase transitions [14,20] and possible dependence of the PPV transition boundary on composition; (2) a convective vigor that is closer to Earth-like; (3) three-dimensional geometry, in which ‘piles’ may turn out to be ridges;

and (4) the formation of seismic anisotropy in the CMB region [28], which could be enhanced by the presence of PPV [16,23]. It would also be useful to investigate the influence of PPV on CMB heat flow and thermal evolution of the Earth's core [19], and the influence of PPV on  $V_s$  and density changes on seismological observations of the deep mantle. Additionally, other material properties such as temperature-dependence of thermal conductivity may influence deep mantle thermal structure and CMB heat flow (e.g., [29]).

## Acknowledgements

The authors thank John Hernlund for constructive discussions, comments and for providing Fig. 2, and Taku Tsuchiya and Dave Yuen for constructive reviews. Financially supported by 21st century COE program for Earth Sciences, University of Tokyo (TN), Grant-in-Aid by MEXT (Wakate-B #17740287) (TN) and US National Science Foundation grant EAR-0207741.

## References

- [1] G. Masters, G. Laske, H. Bolton, A. Dziewonski, The relative behavior of shear velocity, bulk sound speed, and compressional velocity in the mantle: implications for chemical and thermal structure, in: S.-I. Karato, A.M. Forte, R.C. Liebermann, G. Masters, L. Stixrude (Eds.), *Earth's Deep Interior: Mineral Physics and Tomography from the Atomic to the Global Scale*, American Geophysical Union, Washington, DC, 2000, pp. 63–87.
- [2] J. Trampert, F. Deschamps, J. Resovsky, D. Yuen, Probabilistic tomography maps chemical heterogeneities throughout the lower mantle, *Science* 306 (2004) 853–856.
- [3] P.J. Tackley, Three-dimensional simulations of mantle convection with a thermo-chemical basal boundary layer: D"? in: M.M. Gurnis, E.E. Wysession, B. Knittle, A. Buffett (Eds.), *The Core–Mantle Boundary Region*, American Geophysical Union, Washington, DC, 1998, pp. 231–253.
- [4] P.J. Tackley, The strong heterogeneity caused by deep mantle layering, *Geochem. Geophys. Geosyst.* 3 (2002), doi:10.1029/2001GC000167.
- [5] T. Nakagawa, P.J. Tackley, Thermo-chemical structures in the mantle arising from a three-components convective system and implications for geochemistry, *Phys. Earth Planet. Inter.* 146 (2004) 125–138.
- [6] I. Sidorin, M. Gurnis, D.V. Helmberger, Dynamics of a phase change at the base of the mantle consistent with seismological observations, *J. Geophys. Res.* 104 (1999) 15005–15023.
- [7] M. Murakami, K. Hirose, N. Sata, Y. Ohishi, K. Kawamura, Phase transition of MgSiO<sub>3</sub> perovskite in the deep lower mantle, *Science* (2004) 855–858.
- [8] A.R. Oganov, S. Ono, Theoretical and experimental evidence for a post-perovskite phase of MgSiO<sub>3</sub> in Earth's D" layer, *Nature* 430 (2004) 445–448.
- [9] T. Tsuchiya, J. Tsuchiya, K. Umemoto, R.M. Wentzcovitch, Phase transition in MgSiO<sub>3</sub> perovskite in the earth's lower mantle, *Earth Planet. Sci. Lett.* 224 (2004) 241–248.
- [10] J.W. Hernlund, C. Thomas, P.J. Tackley, A doubling of the post-perovskite phase boundary and structure of the Earth's lowermost mantle, *Nature* 434 (2005) 882–886.
- [11] C. Thomas, J. Kendall, J. Lowman, Lower-mantle seismic discontinuities and the thermal morphology of subducted slabs, *Earth Planet. Sci. Lett.* 225 (2004) 105–113.
- [12] C. Thomas, E.J. Garnero, T. Lay, High-resolution imaging of lowermost mantle structure under the Cocos plate, *J. Geophys. Res.* 109 (2004) B08307, doi:10.1029/2004JB003013.
- [13] T. Nakagawa, P.J. Tackley, Effects of a post-perovskite phase change near the core–mantle boundary in compressible mantle convection, *Geophys. Res. Lett.* 31 (2004) L16611, doi:10.1029/2004GL20648.
- [14] P.J. Tackley, S. Xie, STAG3D: a code for modeling thermo-chemical multiphase convection in Earth's mantle, *Proceedings of Second MIT Conference on Computational Fluid and Solid Mechanics*, 2003.
- [15] P.E. van Keken, Cylindrical scaling for dynamical cooling model of the Earth, *Phys. Earth Planet. Inter.* 124 (2001) 119–130.
- [16] U.R. Christensen, D.A. Yuen, Layered convection induced by phase transitions, *J. Geophys. Res.* 90 (1985) 291–300.
- [17] T. Tsuchiya, J. Tsuchiya, K. Umemoto, R.M. Wentzcovitch, Elasticity of post-perovskite MgSiO<sub>3</sub>, *Geophys. Res. Lett.* 31 (2004) L14301, doi:10.1029/2004GL020278.
- [18] J. Tsuchiya, T. Tsuchiya, R. Wentzcovitch, Vibrational and thermodynamic properties of MgSiO<sub>3</sub> postperovskite, *J. Geophys. Res.* 110 (2005) B02402, doi:10.1029/2004JB003409.
- [19] T. Nakagawa, P.J. Tackley, Effects of thermo-chemical mantle convection on the thermal evolution of the Earth's core, *Earth Planet. Sci. Lett.* (2004) 107–119.
- [20] S. Xie, P.J. Tackley, Evolution of helium and argon isotopes in a convecting mantle, *Phys. Earth Planet. Inter.* 146 (2004) 417–439.
- [21] S. Xie, P.J. Tackley, Evolution of U–Pb and Sm–Nd systems in numerical models of mantle convection, *J. Geophys. Res.* 109 (2004) B11204, doi:10.1029/2004JB003176.
- [22] V. Steinbach, D.A. Yuen, W. Zhao, Instabilities from phase transitions and the timescales of mantle thermal evolution, *Geophys. Res. Lett.* 20 (1993) 1119–1122.
- [23] T. Iitaka, K. Hirose, K. Kawamura, M. Murakami, The elasticity of the MgSiO<sub>3</sub> post-perovskite phase in the Earth's lowermost mantle, *Nature* 430 (2004) 442–445.
- [24] F. Deschamps, J. Trampert, P.J. Tackley, Thermo-chemical structure of the lower mantle: seismological evidence and



- consequences for geodynamics. Submitted to *Superplume: Beyond Plate Tectonics*. Submitted for publication.
- [25] T. Irifune, A.E. Ringwood, Phase transformations in subducted oceanic crust and buoyancy relationship at depths of 600–800 km in the mantle, *Earth Planet. Sci. Lett.* 117 (1993) 101–110.
- [26] S. Ono, E. Ito, T. Katsura, Mineralogy of subducted basaltic crust (MORB) from 25 to 37 GPa, and chemical heterogeneity of the lower mantle, *Earth Planet. Sci. Lett.* 190 (2001) 57–63.
- [27] M. Akaogi, A. Tanaka, E. Ito, Garnet–ilmenite–perovskite transitions in the system  $\text{Mg}_4\text{Si}_4\text{O}_{12}$ – $\text{Mg}_3\text{Al}_2\text{Si}_3\text{O}_{12}$  at high pressures and high temperatures: phase equilibria, calorimetry and implications for mantle structure, *Phys. Earth Planet. Inter.* (2002) 303–324.
- [28] A.K. McNamara, P.E. van Keken, S.-I. Karato, Development of finite strain in the convection lower mantle and its implications for seismic anisotropy, *J. Geophys. Res.* 108 (2003), doi:10.1029/2002JB001970.
- [29] C. Matyska, D.A. Yuen, The importance of radiative heat transfer on superplumes in the lower mantle with the new post-perovskite phase change, *Earth Planet. Sci. Lett.* 234 (2005) 71–81.